RESEARCH ARTICLE

Macromolecular Rapid Communications
www.mrc-journal.de

Enhancement of Electrochromic Switching Properties with Tröger's Base-Derived Intrinsic Microporous Polyamide Films

Min-Hao Pai, Chien-Chieh Hu, and Guey-Sheng Liou**

The formation of Tröger's Base (TB) configuration is a useful approach to synthesize polymers of intrinsic microporosity (PIM). Herein, the V-shaped TB scaffold is incorporated to prepare electrochromic (EC) polyamide with electroactive triphenylamine (TPA) moiety. The presence of intrinsic microporosity derived from inefficient packing of TB scaffolds can facilitate the counterions diffusion between electroactive species and electrolytes. Consequently, the resulting TB-based polyamide exhibits enhanced EC behaviors, such as a lower driving potential, reduced the difference of redox potentials ΔE, and shorter switching response time compared to the corresponding EC counterpart polyamide.

1. Introduction

With promising application prospects, EC materials have been in the spotlight and exhibit broad perspectives in countless fields such as anti-glare mirrors, smart windows, electrochromic sunglasses, etc.[1–3] Ideally, an advantaged EC material for practical applications should possess a high color contrast ratio, low driving potential, short switching response, and long cycle life.[2,4,5] However, it is difficult to strike a balance between optical properties and EC behaviors in most cases. For instance, the thicker EC films could display a more obvious color change but result in a longer response time and higher driving potential at the same time due to the obstruction of charge transport including the conveyance of counterions between EC films and electrolytes, and the conduction of electrons in the EC matrix. Recently, our research group has proposed several methods to improve EC behaviors. One is preparing porous EC films via electrolyte salts to promote the diffusion of counterions during the redox procedure,[6] and another is constructing an organic–inorganic hybrid system to facilitate electron transport with the shorter delivery route.[7] In addition, inspired by the enhanced EC properties of the matrix with microporosity, such as covalent organic frameworks (COFs)[8–11] and metal-organic frameworks (MOF),[12–14] the concept of polymers of intrinsic microporosity (PIMs) was also utilized to enhance the switching capability. The H-shaped pentiptycene formation was incorporated to synthesize EC copolymer with intrinsic microporosity, and the outcomes prove the great improvement of response behaviors.[15] However, the incorporation of the non-electroactive pentiptycene-containing diamine monomer would replace the ratio of electroactive *N,N′*-di(methoxyphenyl)-1,4-phenylenediamine (TPPA) and result in EC films with a lower optical contrast ratio. Therefore, how to design and prepare the EC polymers with intrinsic microporosity and maintain optical contrast ratio is a crucial issue for further enhancing response capability.

Recently, polymers with TB scaffold have attracted significant attention due to the unique V-shaped conformation,[16] which hinders the close packing of polymer chains to form the intrinsic microporous structure, and have been applied in various fields such as gas separation[17–21] and ion-exchange membranes.[22–24] Therefore, the contorted and rigid TB scaffold inspires us to synthesize TB-based polymer with intrinsic microporosity as EC material. Herein, the TB-TPA was synthesized as depicted in **Scheme 1**, and the intrinsic microporosity effects derived from TB scaffolds on EC behaviors of triphenylamine (TPA)-based EC polyamide were studied. To investigate the intrinsic microporosity caused by ineffective packing between polymer chains, measurements including wide-angle X-ray diffractometry (WXRD), positron annihilation lifetime spectroscopy (PALS), Brunauer–Emmett–Teller (BET) surface areas, and density were utilized. It is expected that the existence of intrinsic microporosity could facilitate the diffusion rate of counterions between EC films and electrolytes to result in an enhanced EC response capability.

2. Results and Discussion

Two TPA-based polyamides, Ether-TPA and TB-TPA, were prepared by the polycondensation of 4,4′-diamino-4″-methoxytriphenylamine (TPA-OMe) with 4,4′-oxydibenzoic

M.-H. Pai, G.-S. Liou
Institute of Polymer Science and Engineering
National Taiwan University
1 Roosevelt Road, 4th Sec., Taipei 10617, Taiwan
E-mail: gsliou@ntu.edu.tw
C.-C. Hu
Graduate Institute of Applied Science and Technology
National Taiwan University of Science and Technology
No.43, Keelung Rd., Sec.4, Da'an Dist., Taipei 106335, Taiwan
E-mail: cchu@mail.ntust.edu.tw

The ORCID identification number(s) for the author(s) of this article can be found under https://doi.org/10.1002/marc.202100492

DOI: 10.1002/marc.202100492

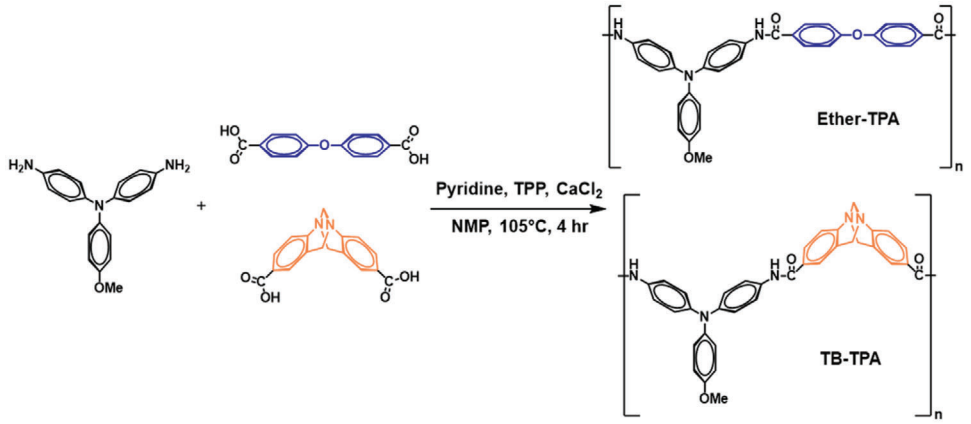

Scheme 1. Synthesis routes of the prepared polyamides.

acid and 2,8-dicarboxy-6H,12H-5,11-methanodibenzo[*b*,*f*][1,5]diazocine (TB-dicarboxylic acid), respectively, as shown in Scheme 1. The ^{1}H NMR and FTIR measurements were used to characterize the structures of these two polyamides as depicted in Figures S1–S3, Supporting Information. The molecular weights and intrinsic viscosities of the polyamides are summarized in Table S1, Supporting Information. Two polyamides with efficient high molecular weight (M_n > 45 000) could form the transparent and flexible films (thickness: 25 ± 5 µm) as demonstrated in Figure S4, Supporting Information. Also, they exhibit excellent solubility in common polar aprotic organic solvents as shown in Table S2, Supporting Information. The thermal properties were carried out by TMA and TGA, and the results are illustrated in Figures S5 and S6 and summarized in Table S3, Supporting Information. Both polyamides exhibit distinguished thermal stability with high decomposition temperatures. Besides, the incorporation of rigid TB scaffolds into the polymer backbone could efficiently increase the softening temperature (T_s) of TB-TPA up to 350 °C, which is 50 °C higher than the counterpart Ether-TPA, owing to the increased stiffness of the polymer backbone.

The characteristics of intrinsic microporosity in the polyamides are depicted in **Figure 1**, and the results are concluded in **Table 1**. First, the density of Ether-TPA and TB-TPA films was measured in 2,2,4-trimethylpentane, and TB-TPA (1.168 g cm^{-3}) revealed a lower density than Ether-TPA (1.193 g cm^{-3}) attributed to the less dense packing of polymer chains in TB-TPA caused by TB scaffolds. The nitrogen adsorption/desorption properties of polymer matrices were conducted at 77 K to support the presence of microporous structure as shown in Figure 1a. Accordingly, the adsorption isotherm of TB-TPA exhibited a more obvious uptake than Ether-TPA. Besides, the estimated BET surface area is three times larger in TB-TPA (50 m^2 g^{-1}) than in Ether-TPA (16 m^2 g^{-1}), confirming the increased microporosity in the polymer matrix of TB-TPA. The pore width distribution also could be verified by the analysis of nitrogen adsorption at 77 K via Horvath–Kawazoe method as illustrated in Figure 1b. As expected, TB-TPA displays more micropores (<2 nm) in the matrix than Ether-TPA. To further investigate the aggregation behavior between the polymer chains, WXRD was measured as depicted in Figure 1c. Both polyamides showed broad amorphous halo patterns with peaks located at ≈2θ = 19° in WXRD, implying some order domain exists in the amorphous polymer matrix. The calculated *d*-spacing is 4.51 and 4.71 Å for Ether-TPA and TB-TPA, respectively, indicating that TB-TPA has the larger interchain distance within the polymer matrix in the out-of-plane direction. Particularly, PALS was used to investigate the characteristics of micropores in the prepared polymer films in this study. The related pore size could be analyzed by the positronium lifetime τ_3 based on the triple-state of positronium (ortho-*Ps*), which is often used to reflect the free volume in polymer materials. As illustrated in Figure 1d, the τ_3 values for TB-TPA and Ether-TPA are 2.194 and 2.173 ns, respectively. Accordingly, TB-TPA displays a higher free volume probability density function (PDF) in the long lifetime side, which is more beneficial for counterions diffusion. Thus, these outcomes demonstrate that a V-shaped TB scaffold is a beneficial configuration to prevent polymer chains from close packing and form more intrinsic microporosity as expected.

The optical properties of the prepared thick films (thickness: 25 ± 5 µm) and thin films coated on indium tin oxide (ITO) glasses were measured by UV–vis spectroscopy. As depicted in Figure S7, Supporting Information, both films showed high transmittance in the visible region, and TB-TPA exhibited higher transparency than the counterpart of Ether-TPA owing to the inhibition of interchain charge transfer (ICT) resulted from the sterically hindered TB scaffolds. The UV–vis spectra and thickness of the thin films are illustrated in Figures S8 and S9, Supporting Information, respectively. The polyamide films with a thickness of ≈600 nm display high transparency in the visible region and are almost colorless, which is beneficial for the EC application.

The electrochemical behaviors of Ether-TPA and TB-TPA films coated on ITO glasses were studied by cyclic voltammetry (CV). The CV diagrams are depicted in Figure S10, Supporting Information, and the results are summarized in **Table 2**. The oxidation potential of TB-TPA (1.10 V) was lower than Ether-TPA (1.14 V). Also, the potential difference between the oxidation and the reduction peaks (ΔE) of TB-TPA was reduced, indicating the lower driving force is enough for the reduction procedure. Accordingly, the TB scaffold demonstrates the positive effects on the enhancement of electrochemical behaviors. This might be attributed to

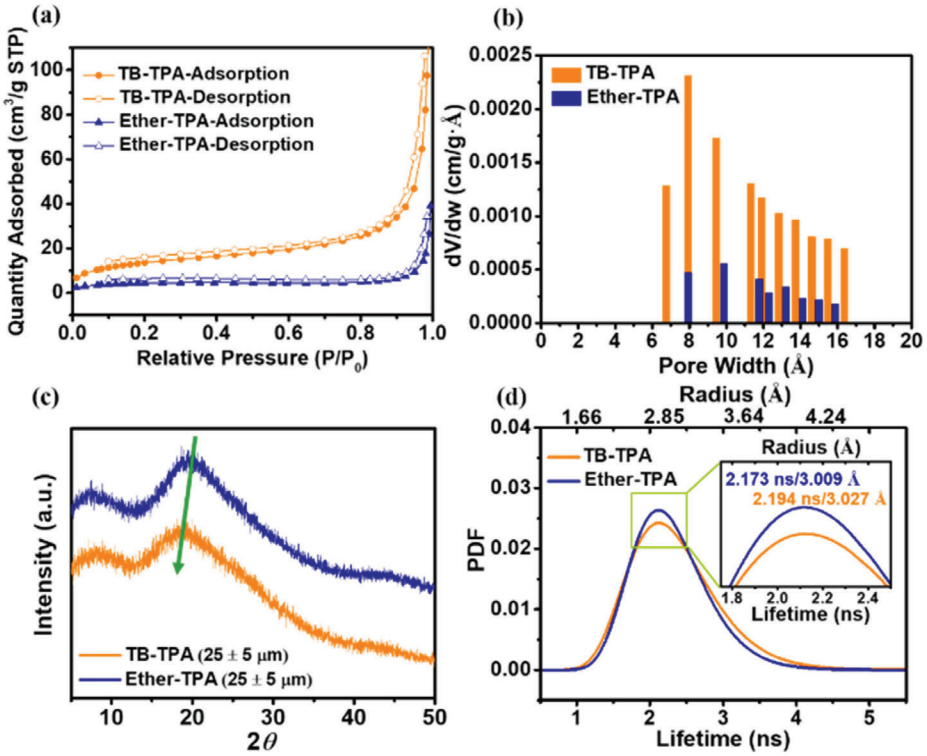

Figure 1. a) N_2 adsorption (filled) and desorption (empty) isotherms measured at 77 K. b) The pore width distribution analyzed by nitrogen adsorption at 77 K via Horvath–Kawazoe method. c) WXRD patterns of polyamide films (thickness: 25 ± 5 μm). d) PALS analysis and calculated pore size.

Table 1. The characteristic of intrinsic microporosity in polyamides.

Polymers	S_{BET} [m^2 g^{-1}][a]	2θ [°][b]	d [Å][c]	ρ [g cm^{-3}]	τ_3 [ns][d]	R [Å][e]
Ether-TPA	16	19.65	4.51	1.193	2.173	3.009
TB-TPA	50	18.83	4.71	1.168	2.194	3.027

[a] Calculated by the results of the N_2 adsorption (filled) and desorption (empty) isotherms measured by BET at 77 K; [b] Measured by WXRD at the scan range of 2θ from 10° to 50°; [c] Calculated from the result of the WXRD curve by Bragg's Law; [d] The *o-Ps* lifetime measured by PALS; [e] The mode radius of free volume size calculated by the result of *o-Ps* lifetime.

Table 2. Electrochemical behaviors of the prepared polyamide films.

Films	$E_{oxi.}$ [V][a]	$E_{red.}$ [V][b]	ΔE [V][c]	R_{ct} [Ω][d]
Ether-TPA (620 ± 30 nm)	1.14	0.43	0.71	71.90
TB-TPA (630 ± 20 nm)	1.10	0.43	0.67	68.46

[a] Oxidation potential at the peak; [b] Reduction potential at the peak; [c] Potential difference between oxidation and reduction peaks, $|E_{oxi.} - E_{red}|$; [d] Obtained from the diameter of the semi-circle or the arc.

the TB scaffolds that prevent polymer chains from close packing and generate intrinsic microporosity, which could lead to a fast counterions diffusion rate within the polymer matrix and explain why the TB scaffold-containing polymer exhibits the lower oxidation potential and smaller reverse reduction driving potential.

Spectroelectrochemical spectra and related *L*, *a**, and *b** values of Ether-TPA and TB-TPA films are shown in Figure S11, Supporting Information, and **Figure 2**a, respectively. Both of the EC films displayed a transparent pale-yellowish color at the neutral state, and exhibit the characteristic absorption peak at 431 and 796 nm corresponding to green color at the oxidation state. Regarding the switching response behaviors, the applied potentials set for coloring and bleaching were 1.15 and −0.1 V, respectively, according to the CV diagram in Figure S10, Supporting Information. As depicted in Figure 2b and **Table 3**, Ether-TPA films required 4.8 and 10.3 s to reach 90% of full switching transmittance changes for coloring and bleaching, respectively. By contrast, TB-TPA films took only 4.3 s for coloring and 9.3 s for bleaching, which was shorter than Ether-TPA. Thus, the higher response-ability of TB-TPA might attribute to the intrinsic microporosity that facilitates the diffusion of counterions between polymer matrix and electrolytes during the redox procedure, and the outcomes agree with the previous report.[15]

Furthermore, electrochemical impedance spectroscopy (EIS) was measured to analyze the conductivity and resistance of the electroactive polymers coated on the electrode.[25] The Nyquist plots of the resulting films are depicted in Figure S12, Supporting Information, and the data analyzed and fitted by the Randles circuit are summarized in Table 2. In general, a lower value of the impedance of charge transfer resistance (R_{ct}) value represents a faster diffusion rate of the counterions. At the coloring potential, the R_{ct} values of Ether-TPA and TB-TPA are 71.9 and 68.46 Ω, respectively, confirming the envisioning again that the effect of intrinsic microporosity on the enhancement of response capability is owing to the improvement of counterions diffusion during the redox procedure.

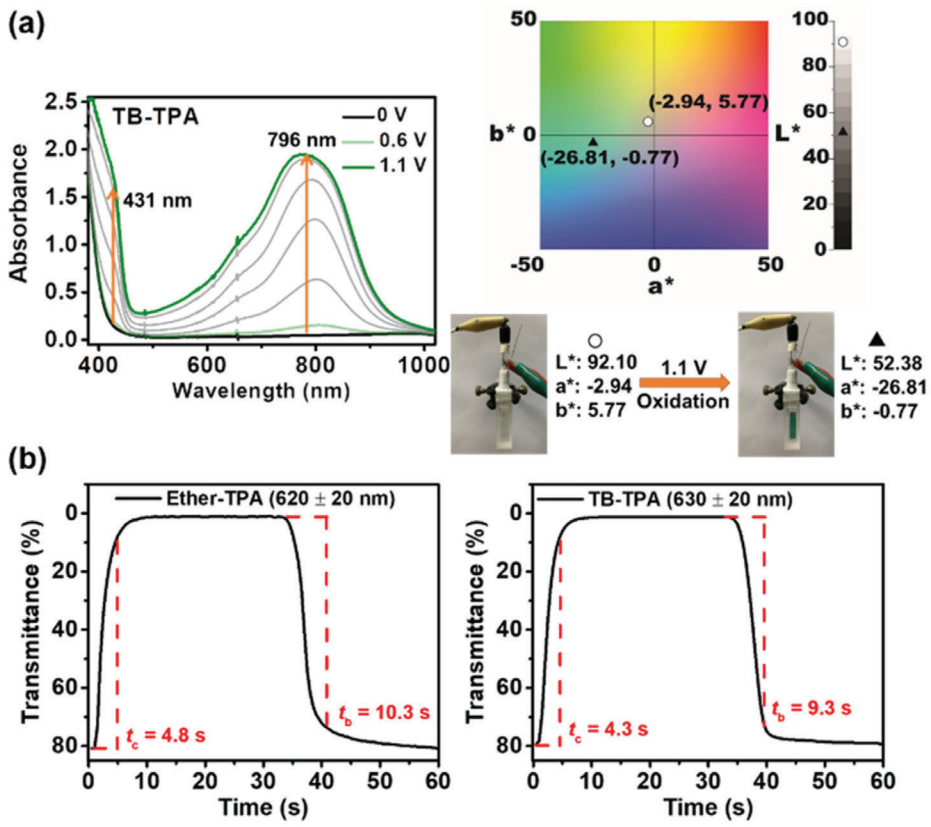

Figure 2. a) Spectroelectrochemical spectra and the CIELAB color space for TB-TPA (thickness: 630 ± 20 nm) measured on the ITO-coated glass substrate in 0.1 M $TBABF_4$/MeCN. b) Switching response time at the wavelength of 796 nm for Ether-TPA (thickness: 620 ± 30 nm) and TB-TPA (thickness: 630 ± 20 nm) on ITO glasses with 1.15 V as coloring voltage and −0.10 V as bleaching voltage in 0.1 M $TBABF_4$/MeCN.

Table 3. EC switching response of the prepared polyamide films.

Films	t_c [s][a]	δt_c [s][b]	δt_c [%][c]	t_b [s][d]	δt_b [s][e]	δt_b [%][f]
Ether-TPA 620 ± 30 nm)	4.8	-	-	10.3	-	-
TB-TPA (630 ± 20 nm)	4.3	0.5	10.4	9.3	1.0	9.7

[a] Coloring time from a neutral state to 90% of optical change; [b] The difference in coloring time compared to Ether-TPA; [c] The percentage of decreasing coloring time compared to Ether-TPA; [d] Bleaching time from coloring state to 90% of the optical change; [e] The difference of bleaching time compared to Ether-TPA; [f] The percentage of decreasing bleaching time compared to Ether-TPA.

The EC devices (ECDs) were fabricated with the incorporation of complementary EC material of heptyl viologen (HV) into gel-type electrolytes for lowering the oxidation potential and enhancing the response. The obtained CV diagrams of the ECDs are shown in Figure S13, Supporting Information, and the results are tabulated in Table S4, Supporting Information. The ECD derived from TB-TPA/HV revealed lower oxidation potential and smaller ΔE (1.26 and 0.26 V) compared to the counterpart device from Ether-TPA/HV (1.27 V, 0.28 V) as the similar tendency of the related EC films. The spectroelectrochemical spectra and related *L*, *a**, and *b** values of TB-TPA/HV and Ether-TPA/HV ECDs are illustrated in Figures S14a and S15, Supporting Information, respectively. The optical absorption spectra of ECDs display the same characteristic absorption peaks as the corresponding EC polyamide films and show an additional characteristic absorption peak of 603 nm for HV^+. Regarding the switching response behaviors at the applied potentials for coloring and bleaching of 1.3 and −0.2 V, respectively, the device of Ether-TPA/HV needed 8.8 and 32.3 s for coloring and bleaching, respectively. In contrast, TB-TPA/HV ECD revealed a shorter response time with only 7.1 s for coloring and 26.5 s for bleaching as depicted in Figure S14b and Table S5, Supporting Information, which are consistent with the trend of the related films, implying the effect of intrinsic microporosity on the enhancement of response capability in ECDs system. Furthermore, the electrochemical stability of TB-TPA/HV ECD was also investigated via CV and spectroelectrochemical measurements as shown in Figures S16 and S17, Supporting Information. Accordingly, TB-TPA/HV ECDs exhibited excellent electrochemical stability even after repeating 1000 redox cycles for CV or spectroelectrochemical cyclic scanning for 10 000 s, indicating the promising potential for practical application.

3. Conclusion

In summary, the TB scaffold-containing EC polyamide has been successfully designed and synthesized for improving the EC behaviors. For the TB-TPA EC film, not only could the oxidation potential be lowered from 1.14 to 1.10 V, but also the response time could be reduced to 4.3/9.3 s for coloring/bleaching steps when

compared to the counterpart Ether-TPA EC film of 4.8/10.3 s. Furthermore, the corresponding ECDs with HV exhibit a similar tendency as the related polyamide films, the oxidation potential of ECD derived from TB-TPA/HV could be lowered to 1.26 V with the switching time of 7.1/26.5 s for coloring and bleaching processes, respectively, which is shorter than the device from Ether-TPA/HV 8.8/32.3 s. This intriguing improvement of EC performance is attributed to intrinsic microporosity formed by the inefficient packing of TB units between polymer chains and provides a feasible concept to design high-performance EC materials for further applications.

Supporting Information

Supporting Information is available from the Wiley Online Library or from the author.

Acknowledgements

This work received financial support from the Ministry of Science and Technology in Taiwan (107-2113-M-002-024-MY3 and 107-2221-E-002-066-MY3).

Conflict of Interest

The authors declare no conflict of interest.

Data Availability Statement

Additional data that supports the findings of this study are available in the supporting information material of this article.

Keywords

electrochromic, intrinsic microporosity, response capability, Tröger's base

Received: July 28, 2021
Revised: August 28, 2021
Published online: October 13, 2021

[1] M. Green, *Chem. Ind.* **1996**, *17*, 641.
[2] R. J. Mortimer, *Chem. Soc. Rev.* **1997**, *26*, 147.
[3] D. R. Rosseinsky, R. J. Mortimer, *Adv. Mater.* **2001**, *13*, 783.
[4] A. A. Argun, P.-H. Aubert, B. C. Thompson, I. Schwendeman, C. L. Gaupp, J. Hwang, N. J. Pinto, D. B. Tanner, A. G. Macdiarmid, J. R. Reynolds, *Chem. Mater.* **2004**, *16*, 4401.
[5] A. L. Dyer, A. M. Österholm, D. E. Shen, K. E. Johnson, J. R. Reynolds, *Electrochromic Materials Devices*, **2015**, 113.
[6] B.-C. Pan, W.-H. Chen, S.-H. Hsiao, G.-S. Liou, *Nanoscale* **2018**, *10*, 16613.
[7] B.-C. Pan, W.-H. Chen, T.-M. Lee, G.-S. Liou, *J. Mater. Chem. C* **2018**, *6*, 12422.
[8] Q. Hao, Z.-J. Li, C. Lu, B. Sun, Y.-W. Zhong, L.-J. Wan, D. Wang, *J. Am. Chem. Soc.* **2019**, *141*, 19831.
[9] S. Xiong, Y. Wang, X. Wang, J. Chu, R. Zhang, M. Gong, B. Wu, Z. Li, *Sol. Energy Mater. Sol. Cells* **2020**, *209*, 110438.
[10] F. Yu, W. Liu, S. W. Ke, M. Kurmoo, J. L. Zuo, Q. Zhang, *Nat. Commun.* **2020**, *11*, 5534.
[11] D. Bessinger, K. Muggli, M. Beetz, F. Auras, T. Bein, *J. Am. Chem. Soc.* **2021**, *143*, 7351.
[12] C. R. Wade, M. Li, M. Dincă, *Angew. Chem., Int. Ed.* **2013**, *52*, 13377.
[13] J. Liu, X. Y. D. Ma, Z. Wang, L. Xu, T. Xu, C. He, F. Wang, X. Lu, *ACS Appl. Mater. Interfaces* **2020**, *12*, 7442.
[14] Z. Zeng, X. Peng, J. Zheng, C. Xu, *ACS Appl. Mater. Interfaces* **2021**, *13*, 4133.
[15] Y.-W. Chiu, W. S. Tan, J.-S. Yang, M.-H. Pai, G.-S. Liou, *Macromol. Rapid Commun.* **2020**, *41*, 2000186.
[16] Ö. V. Rúnarsson, J. Artacho, K. Wärnmark, *Eur. J. Org. Chem.* **2012**, *2012*, 7015.
[17] M. Carta, R. Malpass-Evans, M. Croad, Y. Rogan, J. C. Jansen, P. Bernardo, F. Bazzarelli, N. B. Mckeown, *Science* **2013**, *339*, 303.
[18] Y. Zhuang, J. G. Seong, Y. S. Do, W. H. Lee, M. J. Lee, M. D. Guiver, Y. M. Lee, *J. Membr. Sci.* **2016**, *504*, 55.
[19] Z. Wang, D. Wang, F. Zhang, J. Jin, *ACS Macro Lett.* **2014**, *3*, 597.
[20] Y. Xiao, L. Zhang, L. Xu, T.-S. Chung, *J. Membr. Sci.* **2017**, *521*, 65.
[21] M. Lee, C. G. Bezzu, M. Carta, P. Bernardo, G. Clarizia, J. C. Jansen, N. B. Mckeown, *Macromolecules* **2016**, *49*, 4147.
[22] Z. Yang, R. Guo, R. Malpass-Evans, M. Carta, N. B. Mckeown, M. D. Guiver, L. Wu, T. Xu, *Angew. Chem.* **2016**, *128*, 11671.
[23] J. Zhou, Z. Jiao, Q. Zhu, Y. Li, L. Ge, L. Wu, Z. Yang, T. Xu, *J. Membr. Sci.* **2021**, *627*, 119246.
[24] J. Zhou, Y. Liu, P. Zuo, Y. Li, Y. Dong, L. Wu, Z. Yang, T. Xu, *J. Membr. Sci.* **2021**, *620*, 118832.
[25] M. E. Orazem, B. Tribollet, *Electrochemical Impedance Spectroscopy*, John Wiley & Sons, Inc., Hoboken, NJ **2008**, p. 233.